THE JOURNAL OF PHYSICAL CHEMISTRY B
A JOURNAL OF THE AMERICAN CHEMICAL SOCIETY

pubs.acs.org/JPCB

Article

Investigations of Astrocyte Calcium Signaling and Imaging with Classical and Nonclassical Light

Diletta Spennato,[#] Josephine Leone,[#] Carolyn Gundhardt, Oleg Varnavski, Roberta Fabbri, Marco Caprini, Roberto Zamboni, Valentina Benfenati,* and Theodor Goodson, III*

Cite This: *J. Phys. Chem. B* 2024, 128, 7966–7977

Read Online

ACCESS | Metrics & More | Article Recommendations | Supporting Information

ABSTRACT: The application of light in studying and influencing cellular behavior with improved temporal and spatial resolution remains a key objective in fields such as chemistry, physics, medicine, and engineering. In the brain, nonexcitable cells called astrocytes play essential roles in regulating homeostasis and cognitive function through complex calcium signaling pathways. Understanding these pathways is vital for deciphering brain physiology and neurological disorders like Parkinson's and Alzheimer's. Despite challenges in selectively targeting astrocyte signaling pathways due to shared molecular equipment with neurons, recent advancements in laser technology offer promising avenues. However, the effort to use laser light properties to study astroglial cell function is still limited. This work aims to exploit an in-depth pharmacological analysis of astrocyte calcium channels to determine the physiological mechanism induced by exposure to classical nanosecond-pulsed light. We herein report molecular clues supporting the use of visible-nanosecond laser pulses as a promising approach to excite primary rat neocortical astrocytes and unprecedentedly report on the implementation of entangled two-photon microscopy to image them.

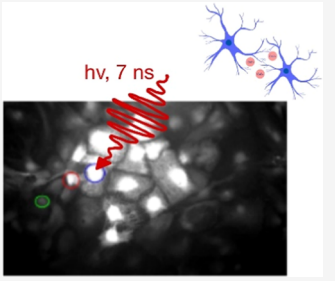

1. INTRODUCTION

The utilization of light for probing living systems and manipulating cellular activity with precise spatial and temporal resolution has been extensively documented in academic literature and remains a major area of scientific investigation.[1−3] The goal of probing living systems with improved temporal characteristics and tighter spatial resolution persists in the fields of chemistry, physics, medicine, and engineering. The nature of the light−matter interaction depends on the properties of the light utilized in the encounter.[4] Thus, the study of the characteristics of photogenic stimulation holds the utmost significance in the realm of biological interventions. Previously published approaches (e.g., optogenetics, photocaging) generally target endogenous or transduced photoactive molecules within cellular structures or utilize light to activate photoactive materials near cell cultures.[5−8] Approaches such as these only indicate the generation of electrical, chemical, or thermal stimuli, which modulate the cell function. Recent studies propose label-free light excitation as a tool for stimulating cells, avoiding the use of exogenously applied or transgenically synthesized fluorophores.[9,10]

Evidence from the past 40 years reveals that the brain's function and ability to receive and convey information rely on the interplay between neurons and non-neuronal cells called glia.[11,12] Among glial cells, astrocytes tightly control the homeostasis of the chemical composition of the extracellular milieu, communicate with neurons modulating synaptic strength, and tune the synchronized ability of neuronal networks to generate brain waves.[13−15] Together, astrocytes demonstrate imperative roles for organ and systemic functions such as learning, memory, behavior, and sleep.[16] Thus, the function of astrocytes is relevant for brain physiology across all spatial-temporal scales. In this regard, a significant interest lies in controlling astrocytes' communication properties, providing mechanistic insights into astrocyte physiology, and elucidating their function at the macroscopic level.[17] With the majority of research focused on the study of light-evoked stimulation/modulation of neurons,[6] there remains a deficit in understanding the interaction between light with different properties and astrocytes.

As nonexcitable cells, astrocytes do not fire action potentials but respond to chemo-physical stimuli through variations in the concentration of intracellular calcium ($[Ca^{2+}]_i$).[18,19] In vivo, astrocytic $[Ca^{2+}]$ ion fluctuations could occur locally, either in so-called microdomains located in the astrocyte's endfeet[20] or in the cell soma or spread over the astroglial syncytium. The temporal dynamics of $[Ca^{2+}]$ ions are complex and depend on the source of calcium generating the $[Ca^{2+}]$ ions. Specifically, intracellular calcium release from the endoplasmic reticulum (ER) and/or extracellular calcium influx concur to $[Ca^{2+}]$ ion genesis and maintenance.[18]

Received: May 17, 2024
Revised: July 18, 2024
Accepted: July 19, 2024
Published: August 12, 2024

https://doi.org/10.1021/acs.jpcb.4c03251
J. Phys. Chem. B 2024, 128, 7966−7977

Notably, differences in calcium signaling mediate different astrocyte functions. As an example, calcium signaling recruiting inositol-3-phosphate receptor (IP3Rs) pathway, located in the endoplasmic reticulum, mediates neurons-astrocytes communication, astrocytic response to sensorial stimulation,[21,22] and $[Ca^{2+}]$ ion signal spreading from one cell to the other through waves. On the other hand, $[Ca^{2+}]$ ions mediated by extracellular influx through members of the transient receptor potential superfamily, such as TRPAnkirin-1 (TRPA1) and TRPVanilloid-4 (TRPV4), are critical for astrocytic control of GABAergic synapse, astroglial regulation of vascular tone, and the response to osmolarity and cell volume changes. Governing a vast scope of homeostatic mechanisms, calcium ion signaling is an effective method for astrocytes to regulate central nervous system (CNS) activity. Accordingly, dysfunction in astroglial $[Ca^{2+}]_i$ pathways was found to be a key factor in the development of many neurological dysfunction disorders, including diseases such as Parkinson's and Alzheimer's.[23−25] It is thus evident that the precise control of distinct molecular signaling pathways of $[Ca^{2+}]$ through tools enabling their selective recruitment is of paramount importance. It represents one of the significant challenges and forefront questions in neuroscience investigation and its application in neurology. However, the expression of similar molecular equipment in neurons and astrocytes hampers selective pharmacology.

Previous attempts using laser light to stimulate and image astrocytes included the use of femtosecond laser stimulation at pulse durations between 80 and 140 fs and wavelengths of approximately 800 nm.[26,27] These methods demonstrated the ability to elicit $[Ca^{2+}]_i$ responses from a variety of cell types, including primary rodent cortical astrocytes. Moreover, pulses of 250 μs duration in the infrared wavelength (1874 nm) exhibit excitation patterns that induce Ca^{2+} responses in rodent astrocytes and neurons in vivo.[28] In the context of methodologies geared toward pharmacological analyses and molecular biology, Borrachero-Conejo et al. demonstrated that $[Ca^{2+}]_i$ responses in primary rodent astrocytes, triggered by a singular 8 ms pulse of infrared laser, involve either external Ca^{2+} influx through TRPV4 and TRPA1 and internal Ca^{2+} release through IP3Rs.[29]

In contrast to other laser techniques employing classical light, pulsed light at the nanosecond time scale mitigates photosensitivity associated with longer pulse durations.[31] The short pulse durations are correlated with greater precision and control over the delivery of laser energy, facilitating a reduced background duration of continuous radiation in cellular plasma.[31] The selective excitation of targeted structures can be utilized to prevent undesired physiological responses in extraneous locations. Additionally, the nanosecond laser generates short pulse durations that avert heat-induced responses after light exposure.[32,33] Given the astrocyte's pronounced temperature sensitivity of Ca^{2+} signals, it is imperative to mitigate type 1 error to determine a correlation between laser exposure and cellular excitation.[33,34] The nanosecond's short interaction time and adequate photon relaxation time mitigate thermal energy dispersion and reduce heat accumulation in astrocytic structures or cellular plasma.[29] In addition to the attributes mentioned above, the nanosecond excitation of astrocytes offers precision and sensitivity, allowing for the integration of nanosecond light as an intriguing prospect in manipulating cellular signaling in vivo[9,30]

Raos et al.[9] initially published the application of nanosecond lasers for the stimulation of Ca^{2+} signals. In their study, human astrocyte samples exhibited an astrocytic Ca^{2+} response upon nanosecond laser light exposure. It was concluded that intracellular calcium release due to the ablation of the endoplasmic reticulum mediated the observed effects. However, further data is needed to correlate the observed effect induced by astrocyte photostimulation with ER calcium release, prompting further research into the implementation of the nanosecond system in biological studies. We coupled the stimulation with a detailed pharmacological analysis to probe the distinct mechanisms activated upon low-energy nanosecond stimulation. With this, the use of technology based on the proposed low-energy nanosecond light stimulation of selective astrocyte calcium pathways might open a new avenue of knowledge on their role in brain function and dysfunction.

Given raised concerns regarding the utilization of high-energy laser pulses for examining astrocyte calcium dynamics, we also explored entangled two-photon microscopy as a novel avenue to enhance imaging efficacy through nonlinear optical signals. Previous studies have validated the capacity of entangled two-photon microscopy to achieve exceptionally low excitation intensities, a feat beyond the capability of classical optical resources.[32,45,46] The entangled light source in the scanning microscope can image biological samples with a significantly lower photon flux compared to classical light sources.[48,46] This decrease in intensity allows for samples imaged with entangled light sources to avoid the damaging effects of phototoxicity and photobleaching.[47]

2. EXPERIMENTAL SECTION

2.1. Primary Cultures of Cortical Astrocytes. Primary cultures of astrocytes were obtained from the cerebral cortex of newborn P0−P2 rats of the Cd Sprague−Dawley genus (Charles River, Italy), using a standard protocol.[49] The experiments were conducted following the regulations of Italian law on protection of laboratory animals, with the approval of bioethical committees of the University of Bologna and of the Ministry of Health (ID 1138, code number 2DBFE.N.3CN, ex-protocol number 360/2017-PR) and under the supervision of the veterinary commission for animal care and comfort at the University of Bologna. Every effort was made to minimize the number of animals used and their suffering. In brief, cerebral cortices were isolated from postnatal rats (P0−P3) or mice (P0−P3), with meninges removed. The tissue was then minced and cultured in flasks with Dulbecco's modified Eagle's medium (DMEM−Glutamax) supplemented with 15% fetal bovine serum (FBS), as well as penicillin−streptomycin (100 U/mL and 100 mg/mL, respectively) from Gibco-Invitrogen, Milan, Italy. Cells were maintained in culture flasks in a humidified incubator (37 °C) with 95% air and 5% CO_2 for 2−5 weeks; the environment is made humid to ensure the buffer system necessary for the cells to survive. After 3 days, the first change of culture medium is made, and from the second week, the medium is changed every 2 days. Upon reaching confluence, usually achieved after about 10−15 days, the cells are ready to be plated for viability and functional assay experiments. This operation begins with trypsinization, the treatment of each flask with 1 mL of 0.4% trypsin (proteolytic enzyme) (Gibco-BRL) and 0.02% ethylenediaminetetraacetic acid (EDTA) (Sigma) to detach the cells from the culture flask. Next, cell counting is continued using Burker's chamber, a hemocytometer representative of the counting chamber. After cell counting, the final volume of the cell suspension is plated on a poly-D-lysine (PDL)-treated

https://doi.org/10.1021/acs.jpcb.4c03251
J. Phys. Chem. B 2024, 128, 7966−7977

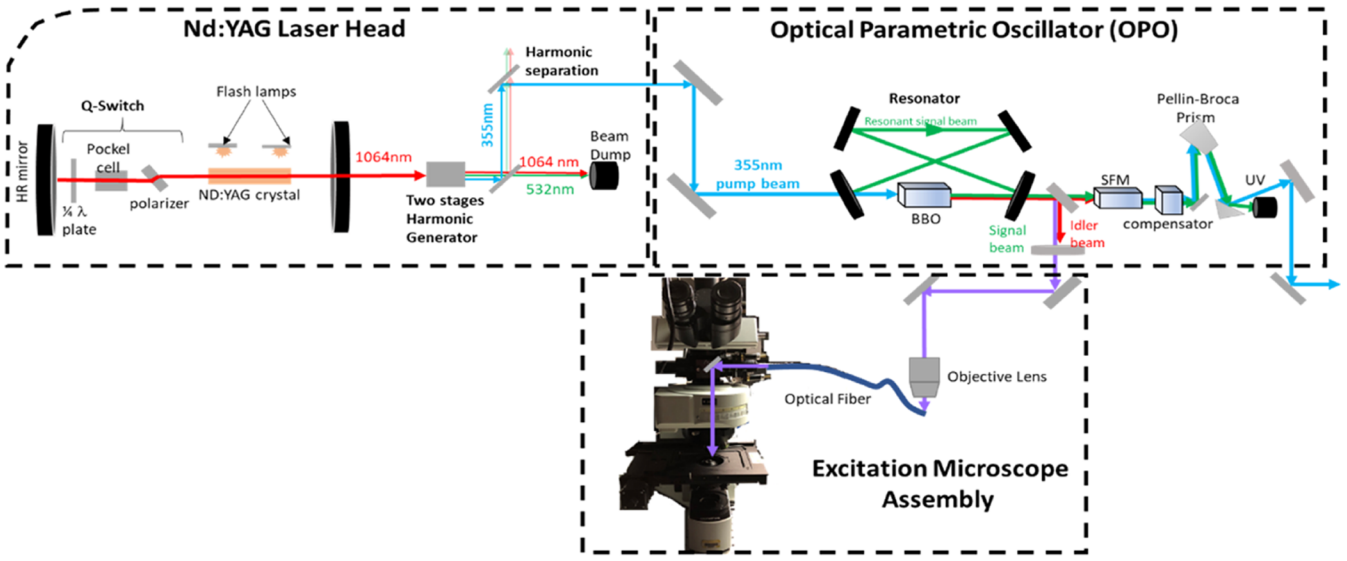

Figure 1. Configuration of the nanosecond laser and the OPO system with microscope.

coverglass. PDL is a chemically synthesized extracellular matrix that facilitates cell adhesion to tissue culture-treated plastic and glass surfaces. Cells are maintained at 37 °C in the CO_2 incubator and observed under the microscope the day after. Plating occurs when the cells reach confluence to maximize their number for the experiment.

2.1.1. Calcium Imaging. Changes in the concentration of free intracellular calcium ($[Ca^{2+}]_i$) were monitored by calcium microfluorimetry using the single-wavelength fluorescent Ca^{2+} indicator Fluo-4 AM (Life Technologies, Milan, Italy) dissolved in a control saline solution. Before measurements, [25 × 10^4] astrocytes per dish were plated on PDL-coated coverslips and loaded with [2 μM] Fluo-4 AM for 45 min. An inverted epifluorescence microscope equipped with a microscopy camera (Thorlabs) was employed to visualize fluorescence-tagged intracellular calcium. All images were captured using a 20× Water Immersion Microscope Objective (Olympus) positioned at the surface of the confocal dish beneath the liquid. Visualization of Fluo-4 was achieved using 480 nm light from a fluorescence excitation lamp, entering the epifluorescence microscope. Before entering the microscope, a 480 nm filter was placed to ensure single-wavelength excitation. The filtered light underwent optical refinement by passing through a beam splitter before reaching the sample. The light produced from Fluo-4 excitation was detected in the sample by a 20× magnified objective lens and recorded by the microscopy camera. A long-pass 500 nm filter was positioned before the camera to mitigate significant light scattering. Data acquisition was executed by using Thorcam software and directed to an external computer for image processing. Camera exposure times were set to 300 ms, with a sampling rate of 2 Hz. The screen scaling provided images that were 575 by 358 μm.

2.2. Nanosecond Excitation Microscopy Analysis. The nanosecond laser induces a transient excited state upon light exposure.[35] When directed toward astrocyte cultures, the nanosecond-pulsed light efficiently converts a high concentration of cells to an excited state, facilitating physiological interactions with adjacent cells.[35,36] As outlined in Figure 1, a spectroscopic QuantaRay neodymium-doped yttrium aluminum (Nd:YAG) laser head was coupled with a GWU optical parametric oscillator (OPO) to produce wavelengths that can be tuned between 250 and 2600 nm. The output beam was adjusted to the visible light region to suit physiological systems. Filters were positioned in the direction of light travel to reduce the administered laser power to optimal conditions. The filtered laser light then entered the objective lens of an epifluorescence microscope equipped with a 0.22 NA optical fiber with a 200 μM core.

By coupling to the optical fiber, light is directed inside the fluorescence microscope. 480 nm light is filtered from mercury to excite Fluo-4 at 485 nm. Additionally, a filter transparent to wavelengths >500 nm is attached before the camera to block out residual 480 nm scattered light. Before reaching the input of the objective lens, the laser light intensity is reduced by a 50/50 beam splitter and a dichroic mirror positioned in the direction of light travel. A comparison of light intensity before and after input into the microscope revealed a reduction of approximately two-thirds, resulting in only about one-third of the light intensity entering the fiber directed toward the samples. Further reductions in excitation energy output may be attributed to variations in beam stability. Consequently, not all of the beam intensity will effectively propagate through the fiber and reach the samples. Laser light entering the optical fiber was measured by using a power meter before entering the microscope. The laser beam used during the experiment to excite cells peaked at 450 nm with high intensity for 1 s = 0.16 J/cm^2 = 1.2 × 10^{19} photons/cm^2.

To conduct each trial, Petri dishes filled with a buffered external solution were placed in position with the optical fiber at the base of the epifluorescence microscope. The laser output was released from the optical fiber and directed toward the cell surfaces with an estimated distance of 220 μM at a 45-deg angle. To control light exposure, a beam blocker was positioned in front of the optical fiber's input, which prevented the laser beam from entering the epifluorescence microscope. For each experimental trial, an area with sufficient astrocyte density was visually identified by using the fluorescence input of the epifluorescence microscope. Before all experimental trials, control tests were conducted by recording calcium dynamics for 4 uninterrupted minutes without introducing laser exposure. Laser light was administered for 1 s, 30 s after

https://doi.org/10.1021/acs.jpcb.4c03251
J. Phys. Chem. B 2024, 128, 7966−7977

the commencement of the experiment, to record the sample's standard state accurately. After laser exposure, experimental trials were extended for an additional 3.5 min to monitor residual calcium fluctuations. To test the intensity and timing of the nanosecond system, we carried out measurements to calibrate the energy and homogeneity of the electric field in the pulse-to-pulse sequences with the nanosecond apparatus shown in Figure 1. For the 7 ns pulses at 450 nm wavelength, the excitation area is 4.7×10^2 μm^2, giving rise to a power density per pulse of 0.16 J/cm^2. In the reported experiments here, 450 nm light was selected for the experimental parameters due to its reduced pulse power and controlled excitation area compatible with biologically sensitive systems (Figure 2).

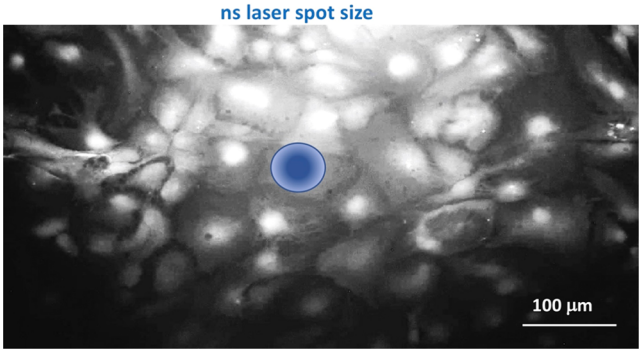

Figure 2. Experimental image size is 575 μm by 358 μm. A bright spot with an excitation area of 4.7×10^2 μm^2 is produced by the nanosecond-pulsed laser light set to 450 nm. Scale bars depict 100 μM.

2.3. Sample Preparation. During the calcium imaging experiments, the standard saline bath solution was used as a control. This solution contained the following concentrations (in mM): 140 NaCl, 4 KCl, 2 $MgCl_2$, 2 $CaCl_2$, 10 *N*-(2-hydroxyethyl)piperazine-*N*′-ethanesulfonic acid (HEPES), and 5 glucose. The pH was adjusted to 7.4 with NaOH, and the osmolarity was adjusted to approximately 318 mOsm by the addition of mannitol. Calcium-free extracellular saline (0 $[Ca^{2+}]_o$) solution contained (mM) the following: 140 NaCl, 4 KCl, 4 $MgCl_2$, 10 HEPES, 0.5 EGTA, pH 7.4 with NaOH, and osmolarity adjusted to ∼318 mOsm with mannitol. The stock solutions of RN-1734 (RN, 10 mM), HC-030031 (HC, 40 mM), and cyclopiazonic acid (CPA, 40 mM) were prepared by dissolving the molecules in dimethyl sulfoxide (DMSO) and then preparing aliquots that were stored at −20 °C. Aliquots of Chembridge (CHE, 100 mM) were prepared in ethanol and stored at a temperature of −20 °C. Aliquots of 2-aminoethoxydiphenylborate (2-APB, 100 mM) were prepared in methanol and stored at −20 °C. Aliquots of ruthenium red (RR, 10 mM) were dissolved in water and stored at −20 °C.

2.4. Statistical Analysis of Dynamical Data. Statistical analyses for calcium imaging experiments were performed with Microcal Origin 8.5. In the detection of calcium imaging, the relationship between the intensity of the fluorescence at each time point (F_t) and the initial fluorescence (F_{t0}), directly related to the variation of $[Ca^{2+}]_i$, was continuously recorded during the experiment. All data are presented as the mean value derived from multiple cells (n) along with the standard error of the mean (SEM). The datasets were subjected to comparison using analysis of variance (ANOVA) followed by the Bonferroni post-test. The data were derived from independent experiments performed at least in triplicate. Regions of interest (ROI) were arbitrarily defined in the cell soma. Fluorescence time series were manually extracted in Metafluor (Molecular Devices, Sunnyvale, CA). Each cell's raw fluorescence intensity was normalized to the mean raw intensity of the 10 frames prior to light exposure, which is reported and analyzed as fractions ($\Delta F_t/F_{t0}$). A cell was defined as "activated" when a 5% increase in normalized fluorescence was observed after light exposure. The fraction of activated cells relative to the total number of cells observed is reported as % of responding cells. The time elapsed to reach the maximal fluorescence intensity after the light stimulus is named "time to peak"; the time required to overcome the response threshold (we set $\Delta F_t/F_{t0} = 0.05$) after the stimulus is referred to as "time onset." To further study calcium dynamics, we counted the "number of peaks" for each cell.

2.5. Entangled Two-Photon Imaging Experiments. Live astrocyte samples were incubated with Hoescht dye to stain the nucleus of each cell. Samples were imaged using a setup consisting of a 405 nm, constant wavelength (CW) laser, and a scanning microscope that included a galvo−galvo scanning head and scanning lenses. The continuous-wave (CW) laser pumped this SPDC unit with 405 nm light, producing a high degree of entanglement frequency.[1] A photon flux of 3.6×10^7 photons/s was generated with an output power of approximately 300 mW from the CW laser. The CW light was directed toward the type-II SPDC unit, which utilized a 1 mm thick β barium borate (BBO) crystal to convert the pumped light from 409 to 818 nm. The resultant images were produced from the detection of this fluorescence signal, which was converted to electrical voltages via a photomultiplier tube and transmitted to the computer system. For initial imaging with the classical light source, a constant wavelength one-photon light set at 408 nm was directed toward fluorescently labeled astrocytes. Excited state emission was recorded to capture the landscape of the cell sample. Subsequently, cells of interest were fixed upon, selected, and magnified for entangled light imaging. The classical imaging utilized a frame size of 1024 × 1024 pixels and a pixel binning factor (PBF) of 100, while the entangled image was captured in complete darkness with a frame size of 128 × 128 pixels and a PBF of 400. The entangled image accumulated 3000 recorded frames.

3. RESULTS

3.1. Nanosecond Excitation at 450 nm of Primary Cortical Astrocytes' Calcium Signaling In Vitro. The nanosecond laser produced 450 nm visible light with 7 ns pulses. When fixed according to these parameters, the nanosecond system operated at a power density of 0.16 J/cm^2 per pulse. In previously reported experiments, pulsed infrared light was employed to elicit calcium signaling in astrocyte cells at a high photon flux and energy intensity of 14.31 J/cm^2.[2,4,9,37] Compared to the previously reported infrared techniques, we observed astrocytic excitation at a photon intensity of 2 orders of magnitude lower.[38−394041]

The magnitude of Fluo-4 fluorescence intensity, which directly correlates with the variation in $[Ca^{2+}]_i$, was recorded before, during, and after ns laser stimulation (Figure 3). The traces reported in Figure 3 represent the baseline fluorescence recorded before (Figure 3c) and after a 450 nm laser pulse was delivered to the cells (Figure 3d). Notably, a strong $[Ca^{2+}]_i$ peak was reported upon nanosecond-pulsed light exposure

https://doi.org/10.1021/acs.jpcb.4c03251
J. Phys. Chem. B 2024, 128, 7966−7977

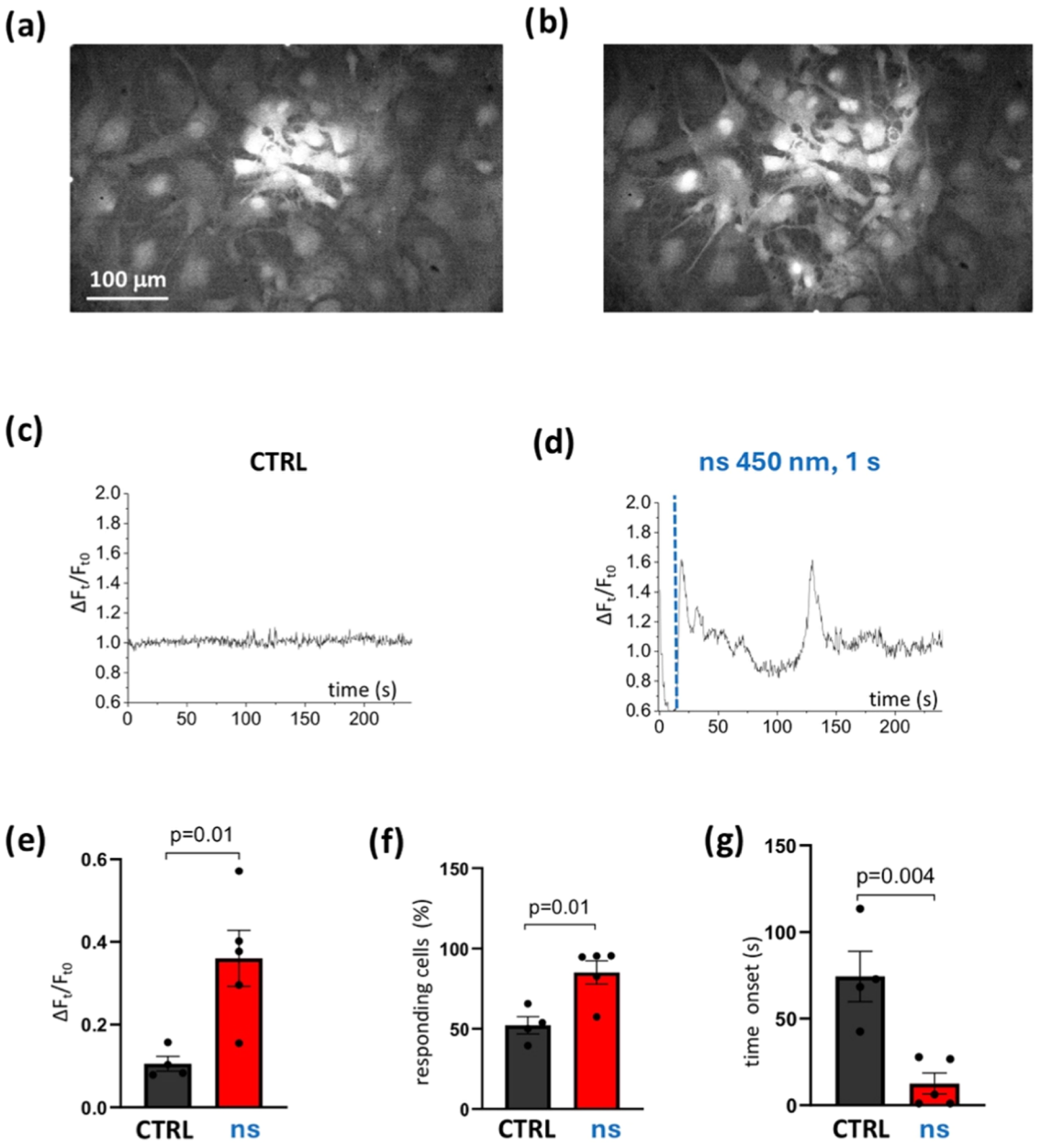

Figure 3. 450 nm nanosecond laser stimulation induces $[Ca^{2+}]_i$ signaling responses in primary astrocytes. (a) Fluorescent image of rat astrocytes loaded with Fluo-4 before and after (b) stimulation with ns laser pulse (1 s). Representative traces of Fluo-4 fluorescence variation over time ($\Delta F_t/F_{t0}$) monitored in the control condition (c) or when astrocytes are exposed to a 450 nm laser stimulation (d). The dashed blue line in panel (d) represents the time point at which the ns laser pulse was delivered. (e) Bar plots depicting the average peak of variation in fluorescence observed before (black bar) and after exposure to a nanosecond pulse laser (red bar). (f) Percentage of responding cells to ns laser stimulation, with a response threshold set to $\Delta F_t/F_{t0} > 0.05$. (g) The time onset of the calcium response in the observed dynamics. All data described in the histograms are reported as mean ± SEM. ANOVA−Bonferroni test is executed on data groups, $^*p < 0.05$, $^{**}p < 0.01$, and $^{***}p < 0.001$.

followed by a long-lasting response (time onset ctrl: 74.3 ± 13.7 s vs time onset ns laser: 12.5 ± 5.6 s). In some experimental trials, further $[Ca^{2+}]_i$ peaks were observed following the initial peak before returning to the baseline after hundreds of seconds. Statistical analysis revealed that the average increase in fluorescence intensity was significantly higher in nanosecond-stimulated astrocytes ($\Delta F_t/F_{t0}$ ns laser: 0.36 ± 0.04) than that measured in the control condition ($\Delta F_t/F_{t0}$ ctrl: 0.11 ± 0.01) (Figure 3d). Our results show that 80% of the astrocytes respond to nanosecond laser stimulation (% responding cells ctrl: 52.2 ± 5.36 vs % responding cells ns laser: 85.14 ± 7.35; response threshold $\Delta F_t/F_{t0} > 0.05$, Figure 3f).

Figure 4 illustrates the interactions between three adjacent cells before and after 450 nm ns laser exposure. Time 0 represents the baseline cellular fluorescence, which was used to eliminate background fluorescence for the following images. The progression of the images, along with the standardized graph of cellular fluorescence ($\Delta F/F_0$), indicates that increases in astrocyte $[Ca^{2+}]_i$ concentration propagate among adjacent cells following nanosecond-pulsed light exposure. Notably, following ns exposure, an increase in fluorescence is initially recorded in cells directly targeted by the laser, followed by an

https://doi.org/10.1021/acs.jpcb.4c03251
J. Phys. Chem. B 2024, 128, 7966−7977

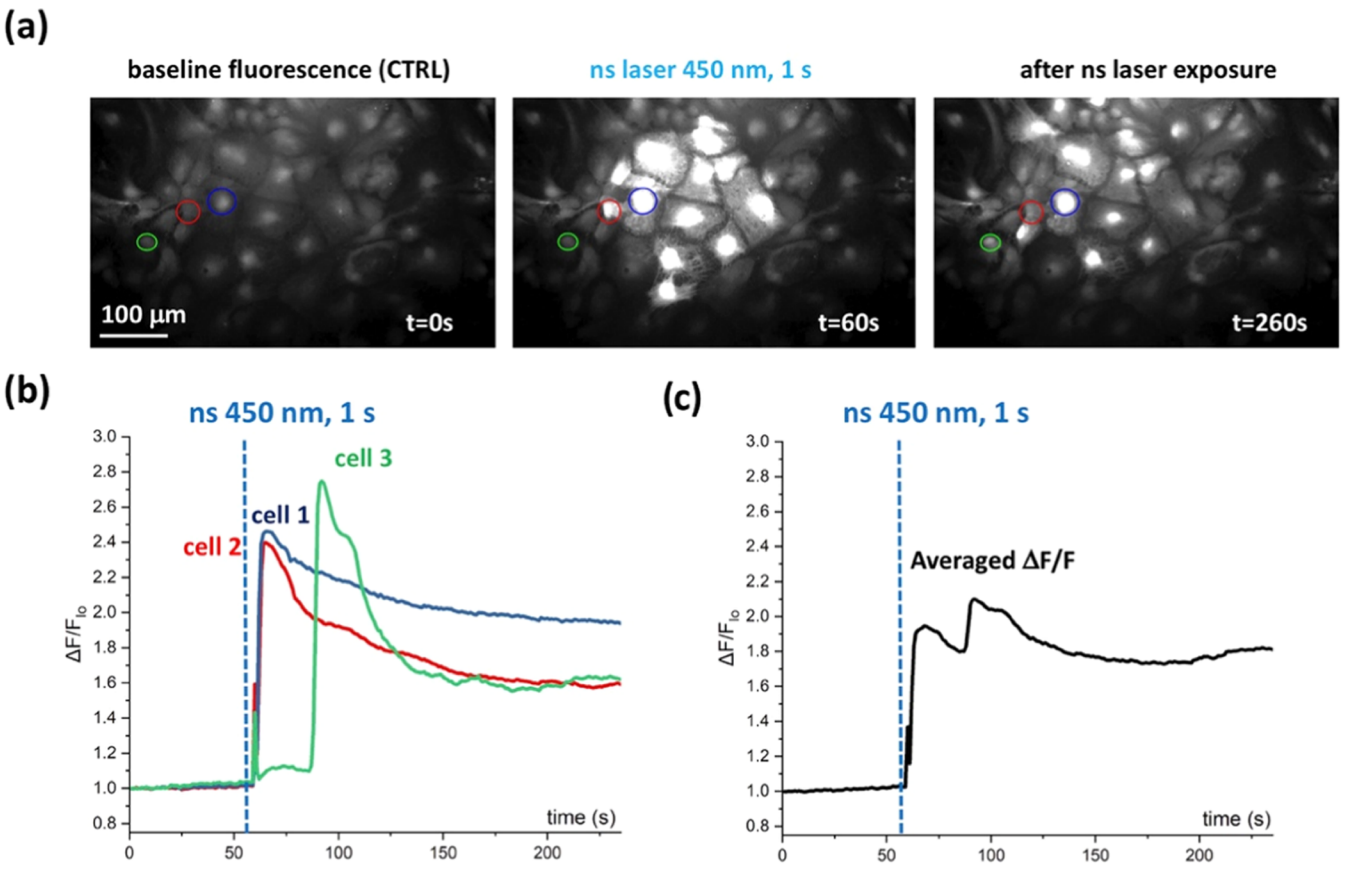

Figure 4. (a) Fluo-4 labeled fluorescent astrocytes visualized within the image frame are visually shown over a 240-s time scale. Round circles represent regions of interest (ROI) that were graphically displayed in panel (b) with their corresponding trace color. (b) The fluorescence intensity variation over time ($\Delta F/F_0$) of three individual cells is presented as graphical traces over 240 s. Each cell is represented by a different color. Interactions between individual cells are displayed evidently by time lag between onset of the traces. (b) The average fluorescence intensity ($\Delta F/F_0$) of all cells in the image frame is graphically presented over a 240 s time scale. The increase in fluorescence intensity is shown after laser light exposure and decreases after the significant peak is reached (c).

increase in fluorescence radiating outward to adjacent cells. This relationship is further supported by the experimental images (Figure 4a), which depict localized fluorescence radiating from the excitation point.

The average change in fluorescence intensity for all cells within the video frame (575 μm by 358 μm) demonstrates similar trends to what was analyzed at the singular cell level. The peaks in fluorescence intensity were significantly elevated from baseline, followed by a gradual decline (Figure 4b). The average fluorescence intensity shows that networks of astrocytes maintain a transient excited state for prolonged durations following nanosecond laser exposure (Figure 4b). Prior to returning to baseline fluorescence, the sample's average fluorescence fluctuates between high and low fluorescent states. The typical pattern of fluorescence excitation peaks is presented as an isolated cell over 240 s (Figure 4b,c).

3.2. Pharmacology of the Astrocytic $[Ca^{2+}]_i$ Response to ns Laser Pulse. Our results address a significant piece of information that is missing in the understanding of the source of $[Ca^{2+}]_i$ in astrocytes stimulated by nanosecond laser pulses. We filled this gap by performing a detailed pharmacological analysis of the response we observed to the 450 nm, 1 s, ns laser pulse. First, we aim to verify the role of intracellular calcium release from intracellular organelles such as the endoplasmic reticulum and mitochondria.

Figure 5 reports the traces and analysis recorded for each compound tested condition. First, an extracellular solution that did not contain Ca^{2+} was used to impede the influx of extracellular Ca^{2+} into astrocytes' cytoplasm. Here, we found that the magnitude $\Delta F_t/F_{t0}$, thus the amplitude of the $[Ca^{2+}]_i$ response to ns pulsed light, and the percentage of responding cells were comparable to the data obtained in control saline (Figure 5f,g light blue bars—$\Delta F_t/F_{t0}$ ctrl ns laser: 0.35 ± 0.02 vs $\Delta F_t/F_{t0}$ 0 $[Ca^{2+}]_o$: 0.41 ± 0.04, % responding cells ctrl ns laser: 85.14 ± 7.35 vs % responding cells 0 $[Ca^{2+}]_o$: 95 ± 5). However, the onset of the response, the time to peak, and the number of peaks were significantly reduced (Figure 5h–j, light blue bars; time onset 0 $[Ca^{2+}]_o$: 12.9 ± 4.7 s, time to peak 0 $[Ca^{2+}]_o$: 47.8 ± 10.7 s, number of peaks 0 $[Ca^{2+}]_o$: 1.87 ± 0.13). These results indicate that extracellular calcium is not essential for a localized increase in $[Ca^{2+}]_i$ following the nanosecond laser pulse but could be implicated in its dynamics, which are slower and show repetitive peaks only when external calcium is present.

Second, we tested the effect of 2-APB on trials in conjunction with control saline. 2-APB is a functional and membrane-permeable D-myo-inositol 1,4,5-trisphosphate (IP3) receptor antagonist that blocks the IP3Rs pathway. We found that the presence of 2-APB resulted in a significant decrease in the intensity of the fluorescent response after exposure to the ns laser pulse, $\Delta F_t/F_{t0}$: 0.15 ± 0.03 (Figure 5f, violet bar). The

https://doi.org/10.1021/acs.jpcb.4c03251
J. Phys. Chem. B 2024, 128, 7966−7977

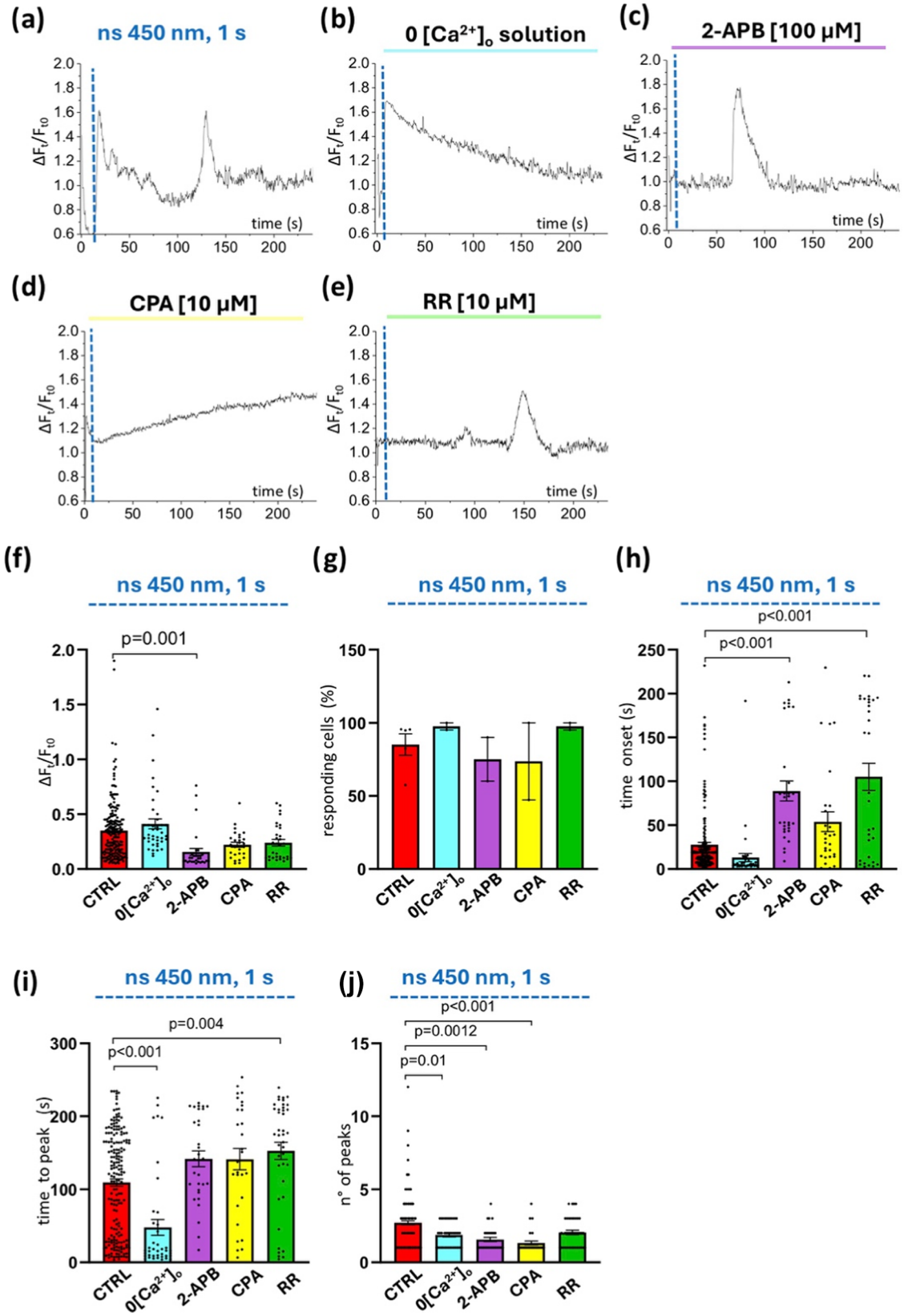

Figure 5. Pharmacological analysis of $[Ca^{2+}]_i$ signaling in ns laser-stimulated astrocytes. (a−e) Representative traces of calcium imaging experiments were performed in different conditions where specific solutions and drugs were applied during the ns laser stimulus (450 nm, 1 s). Blue dashed lines indicate the specific time point when the nanosecond laser pulse was delivered. (a) Astrocytes are stimulated with ns laser 450 nm in standard saline, which is used as control (CTRL); (b) astrocytes are bathed with extracellular solution not containing calcium (0 $[Ca^{2+}]_o$); (c) typical trace recorded adding 2-APB, 100 μM, to the extracellular solution. (d) Representative trace of experiments performed with saline solution added with CPA, 10 μM, and (e) RR, 10 μM; (f) bar plot reporting averaged mean of the maximum fluorescence increments measured when cells are immersed in a 0 $[Ca^{2+}]_o$ solution (light blue column) or when adding 2-APB (violet column) or CPA (yellow column) or RR (green column).

https://doi.org/10.1021/acs.jpcb.4c03251
J. Phys. Chem. B 2024, 128, 7966−7977

Figure 5. continued

(g) Bar plot the percentage of astrocytes exceeding the response threshold ($\Delta F_t/F_{t0} > 0.05$) in different conditions tested: 0 $[Ca^{2+}]_o$ light blue column, adding 2-APB (violet column) or adding CPA (yellow column) or RR (green column) to the control saline. (h−j) Bar plots reporting results of analysis of $[Ca^{2+}]_i$ temporal dynamics: averaged time onset of the response (h), time to peak (i), and the number of peaks (j). The conditions tested are astrocytes bathed with a solution not containing extracellular calcium (0 $[Ca^{2+}]_o$, light blue bars); saline solution with 2-APB (violet bars) or CPA (yellow bars) or RR (green bars). Dashed blue line cells indicate that astrocytes were triggered with ns laser pulse. All data described in the histograms are reported as mean ± SEM. ANOVA−Bonferroni test is executed on data groups, $*p < 0.05$, $**p < 0.01$, and $***p < 0.001$.

presence of 2-APB also significantly decreased the number of peaks: *n* peaks: 1.56 ± 0.14 (Figure 5j, violet bar). Additionally, with respect to the temporal dynamics of $[Ca^{2+}]_i$, the onset of the response was largely delayed by 2APB (t_{onset} 2-APB = 88.8 ± 11.37 s vs t_{onset} ns laser = 12 ± 5.6 s, Figure 5h, violet bar). However, experimental trials with 2APB did not significantly affect the percentage of responding cells (% responding cells 2APB: 75 ± 15), (Figure 5g, violet bar), and time to peak data did not display a significant difference from control trials (*t* peak 2APB: 141 ± 10 s vs *t* peak ns laser: 90 ± 10 s).

Third, endoplasmic reticulum Ca^{2+}-ATPase (SERCA) is an important Ca^{2+} source in intracellular calcium signaling, mainly involved in store-operated Ca^{2+} entry in astrocytes. In order to test the significance of SERCA in the response to ns pulsed light, CPA, a reversible inhibitor of SERCA, was used in conjunction with control saline. The data demonstrate that the addition of CPA does not significantly alter $\Delta F_t/F_{t0}$, the percentage of responding cells, or the time to peak (Figure 5f,g,i yellow bars; $\Delta F_t/F_{t0}$ CPA: 0.22 ± 0.02, % responding cells CPA: 73.6 ± 26.3, time to peak CPA: 141 ± 14 s). However, in the presence of CPA, the onset of the response shows a significant delay, and the number of peaks was significantly reduced (Figure 5h,j yellow bar; time onset CPA: 53.8 ± 11 s, the number of peaks CPA: 1.32 ± 0.14).

Fourth, ruthenium red (RR) was used to block the uptake and release of calcium from the mitochondria and its release from ryanodine-sensitive intracellular stores as well as to serve as a nonspecific inhibitor of TRP channels. The presence of RR in conjunction with control saline delayed both the onset of the response to the ns laser stimulation, t_{onset} RR 100 ± 15 s, and the time to peak, t_{peak} RR 152 ± 11 s (Figure 5h,I, green bars), whereas $\Delta F_t/F_{t0}$, the percentage of responding cells, and the number of peaks did not show significant change (Figure 5f,g,j, green bars; % responding cells RR: 95 ± 5, *n* peaks RR: 2 ± 0.15).

Given the importance of extracellular calcium influx in astrocyte physiology and in their response to other laser pulse sources, such as infrared light, we next investigated the possible involvement of TRP calcium-permeable channels in this phenomenon. We focused particularly on TRPA1 and TRPV4, which are highly expressed in astrocytes.

Figure 6 reports representative traces of calcium imaging experiments in which the fluorescence intensity is proportional to the calcium concentration. The astrocyte's fluorescence intensity was measured before, during, and after the delivery of the nanosecond laser pulse (450 nm, 1 s, 33.55 J) (Figure 6a). Additionally, the same experiment was repeated with specific inhibitors targeting TRPA1 (Figure 6b,c) and TRPV4 (Figure 6d) added to control saline.

Our data demonstrate that the selective blockers of the TRPA1 channel, HC030031 (HC) and Chembridge (CHE), produce a comparable percentage of responding cells to control conditions (% responding cells HC: 94 ± 5, responding cells CHE: 96 ± 3 vs % responding cells ns ctrl condition: 85 ± 7.35). Additionally, the time onset and number of peaks did not change significantly; (time onset HC: 8.48 ± 1 s, time onset CHE: 12 ± 1.58 vs time onset ctrl ns laser: 25 ± 2.5; *n* peaks HC: 1.95 ± 0.05, *n* peaks CHE: 2.4 ± 0.15 vs *n* peaks ctrl ns: 2.5 ± 1) (Figure 6g,i). While the intensity of the response was significantly elevated for trials under HC conditions ($\Delta F_t/F_{t0}$ HC: 0.84 ± 0.07), trials under CHE conditions were not significantly elevated ($\Delta F_t/F_{t0}$ CHE: 0.46 ± 0.03) (Figure 6e, orange and purple bars). Interestingly, the time to peak was shortened by the application of inhibitors of TRPA1 (Figure 6h, orange and purple bars, time to peak CHE: 40 ± 8 s time to peak HC: 14 ± 4 s vs time to peak ns laser ctrl: 100 ± 6 s). Considering these data, the findings indicate that TRPA1 is not the channel responsible for the increase in intracellular calcium measured in astrocytes after ns laser excitation. Although HC trials displayed a shortened time to peak and elevated fluorescence, the lack of elevated fluorescence in CHE trials and no change in the number of responding cells under both HC and CHE conditions support this conclusion.

To identify the role of the TRPV4 channel in this phenomenon, we also added its selective antagonist, RN-1734, to the standard solution. Of the various parameters analyzed, $\Delta F_t/F_{t0}$, percentage of responding cells, time to peak, and number of peaks did not show significant change with respect to the response to ns laser pulse recorded in standard saline conditions (Figure 6e,f,h,I, green bars, $\Delta F_t/F_{t0}$ RN: 0.27 ± 0.03, % responding cells RN: 84 ± 16: time to peak RN: 98 ± 12 s, *n* of peaks RN: 2 ± 0.18 vs ns laser condition). However, we note a delay in the onset of the response (Figure 6g, green bar, time onset RN: 35 ± 9 s)

4. DISCUSSION

Our data present that in live astrocyte cells, nanosecond-pulsed laser stimulation at 450 nm induces exclusively intracellular calcium rises. Additionally, in the results reported in this contribution, we show the molecular pathway underpinning the observed effect. It is concluded that the target of laser stimulation is the endoplasmic reticulum and, particularly, IP3Rs. A similar hypothesis was suggested by Raos et al. where nanosecond UV laser light was used to induce an intracellular calcium response in astrocyte cells; Raos and colleagues describe how nanosecond UV laser pulses (wavelength of 365 nm) can induce $[Ca^{2+}]_i$ responses in human hNT astrocytes.[9] However, their research indicates that the main stimulus for the $[Ca^{2+}]_i$ response is the localized ablation of the ER with the use of 4.512 μJ light, differing from our results. More specifically, they suggest that the $[Ca^{2+}]_i$ responses elicited by UV nanosecond laser pulses are due to ablation of the ER, leading to a localized increase in calcium levels within the cytoplasm. This localized increase in $[Ca^{2+}]_i$ is transmitted

https://doi.org/10.1021/acs.jpcb.4c03251
J. Phys. Chem. B 2024, 128, 7966−7977

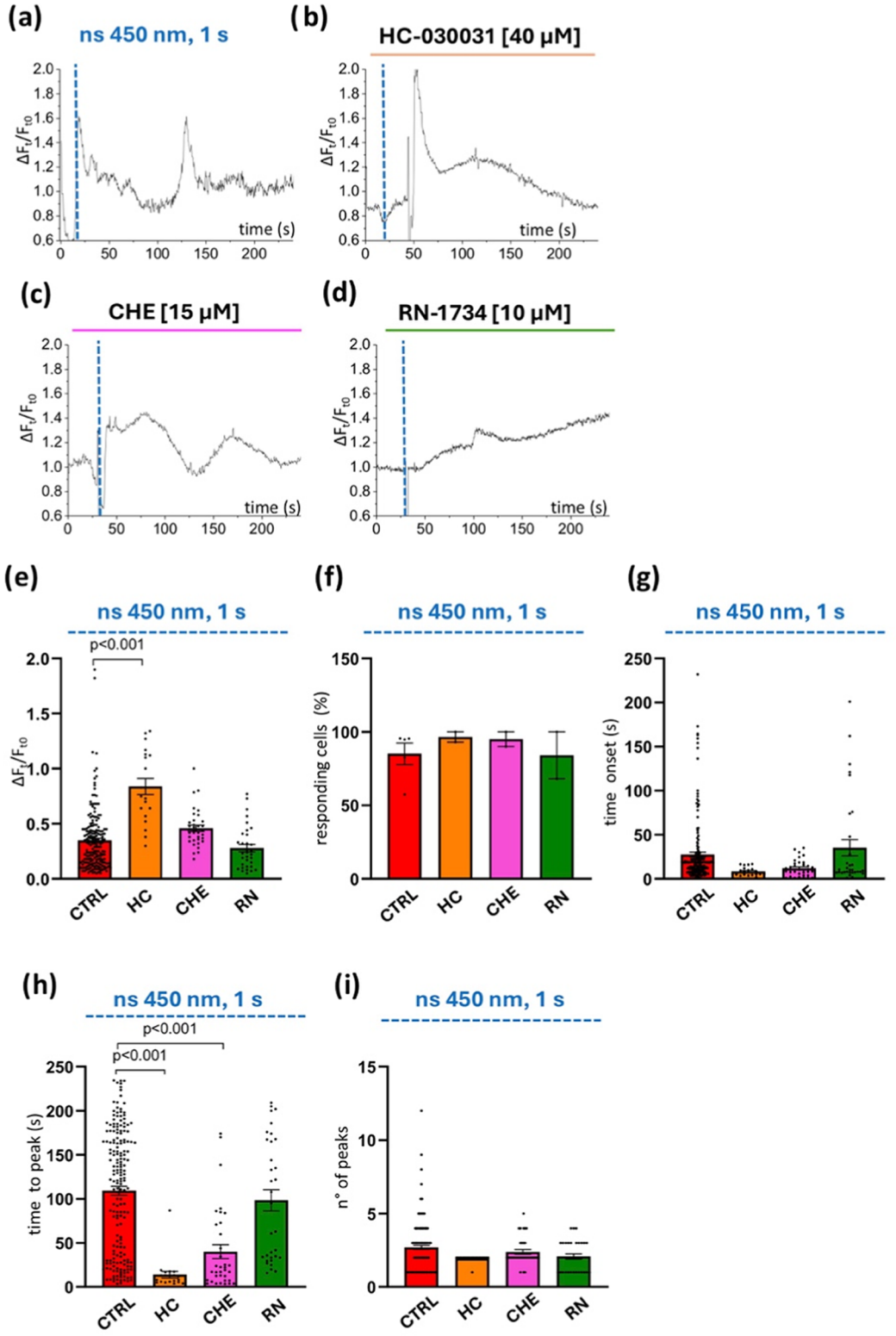

Figure 6. EXT-Ca^{2+} influx through TRPPs is not induced by ns laser pulse. (a–d) Typical traces of calcium imaging experiments, performed in different conditions where specific drugs are applied after ns laser stimulus (450 nm, 1 s). The blue dashed line marks the specific time point when the nanosecond laser pulse was delivered. (a) Astrocytes are stimulated with ns laser 450 nm in standard solution; (b) after the addition of TRPA1 selective blockers HC-030031 [40 μM] or (c) Chembridge (CHE) [15 μM]; (d) after addition of RN-1734 [10 μm], a TRPV4 blocker. Bar plots reporting the average of the mean of the maximum fluorescence increments (e), the percentage of responding astrocytes (f), time onset of the response (g), time to peak (h), and the number of peaks (i). The conditions tested were as follows: saline + HC (orange bars), + CHE (purple bars), or + RN (green column). In all cases, cells were first triggered with ns laser pulse (dashed blue line). The red columns of each graph represent the control condition where cells were stimulated with ns laser in a standard solution. All data described in the histograms are reported as mean ± SEM. ANOVA–Bonferroni test is executed on data groups, *$p < 0.05$, **$p < 0.01$, and ***$p < 0.001$.

https://doi.org/10.1021/acs.jpcb.4c03251
J. Phys. Chem. B 2024, 128, 7966–7977

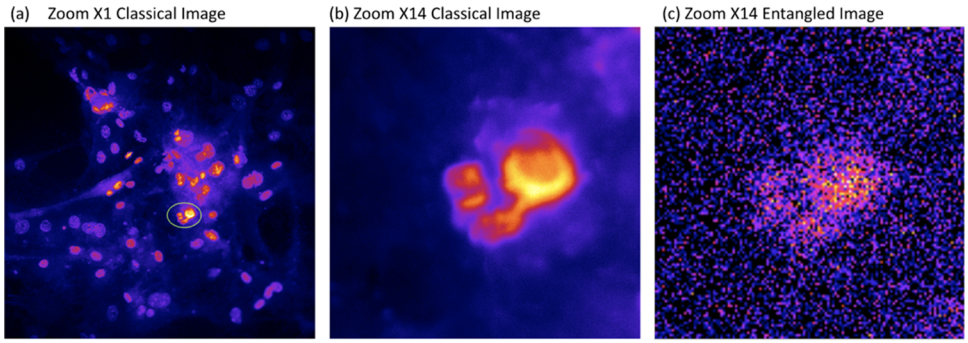

Figure 7. (a) One frame of classical one-photon 409 nm light directed toward astrocyte samples at Zoom X1 (770 μm × 770 μm). (b) One frame of classical one-photon 409 nm light directed toward astrocyte samples at Zoom X14 (55 μm × 55 μm). (c) 3000 accumulated frames of entangled two-photon 818 nm light directed toward the Hoechst-stained astrocyte sample at Zoom X14 (55 μm × 55 μm).

throughout the cell via calcium-induced calcium release (CICR). The idea of site-specific stimulation thresholds may also explain the observation that some astrocytes were initially unresponsive upon exposure to low-energy beams but later became responsive upon exposure to higher-energy pulses. The hypothesis suggests that the $[Ca^{2+}]_i$ response in neighboring cells is a consequence of intercellular communication with the laser-stimulated cell.[9] Our work unequivocally shows that IP3Rs are elicited with photogenic stimulation. Our pharmacological analysis supports the conclusion that intracellular stores release calcium following laser excitation, not by destroying (ablating) them but by activating a specific pathway on the endoplasmic reticulum that mediates calcium release.

Additional support for the hypothesis of involvement of IP3Rs could be found in recent research by Li et al. in 2023.[30] Using a methodical chip model, the study applied repetitive UV laser stimulation to a structured network of 5 × 5 hNT astrocyte stellate cells. This study showed that the propagation of $[Ca^{2+}]_i$ waves was significantly hindered when suramin, an ATP receptor antagonist, was applied. Interestingly, the chemical blockade of gap junctions had no significant effect on $[Ca^{2+}]_i$ wave propagation. These findings strongly suggest that ATP, rather than gap junction channels, serves as a mediator for the transmission of UV laser-induced intracellular $[Ca^{2+}]_i$ signaling in hNT astrocytes, particularly within neighboring and next-neighbor regions of organized networks. ATP binding to membrane-bound receptors leads to the generation of IP3, which triggers the release of intracellular Ca^{2+} from Ca^{2+} stores.[30]

Mellor and co-workers focused their experimental studies on glioblastoma (GBM), the most common and lethal form of high-grade brain cancer in adults. They found that laser-stimulated $[Ca^{2+}]_i$ transients can travel between cells up to 200 μm from the source cell. The stimulation pathway was proven to involve the endoplasmic reticulum (ER). Excitation was abolished, as demonstrated by testing with thapsigargin, a potent inhibitor of the ER Ca^{2+} ATPase pump.[42] TRPA1 and TRPV4 do not appear to be involved in the nanosecond laser-dependent calcium response we observed. This is interesting because it demonstrates that TRPA1 and TRPV4 channels were instead critical in the response to infrared laser pulses. Infrared (IR) lasers generate thermal transients that can stimulate neurons in both the central and peripheral nervous systems.[10,43] Moreau et al. used IR free-electron laser in the rat sciatic nerve.[44] Here, they showed that the mechanism of INS is based on transient and localized heating caused by the absorption of IR light by water molecules.[44] INS is an effective method to excite action potentials in neurons. However, in primary astrocytes, an 8 ms infrared laser pulse (1875 nm) alters the biophysics of the plasma membrane without destroying it and causes changes in the cell volume. Calcium imaging studies showed that the TRPA1 channel is activated and incoming calcium activates the release of more calcium from intracellular organelles (IP3R-dependent). The increase in $[Ca^{2+}]_i$ stimulates TRPV4 and makes it sensitive to changes in cell volume. The stimulated calcium dynamics propagate between cells via gap junctions.[29]

5. CONCLUSIONS AND OUTLOOK

This contribution provides an in-depth pharmacological analysis in conjunction with low-intensity nanosecond techniques. We have demonstrated that nanosecond visible light may be utilized at pulse energies 2 orders of magnitude lower than previously used infrared techniques to trigger calcium signaling pathways in astrocytes.[29] The pharmacological analysis proved that upon exposure to 450 nm, nanosecond-pulsed light, astrocyte excited state dynamics depend on intracellular calcium release, specifically at IP3R channels. This poses significance in the development of techniques capable of neurological excitation with parameters safe for in vivo use.

Collectively, the results indicate that astrocytes can be excited by low-intensity nanosecond pulse stimulation. A thorough pharmacological analysis was performed, revealing that external Ca^{2+} influx is not a determinant for the onset and the magnitude of the response but for sustaining the response over time. Regarding intracellular calcium ion release, we conclude that the endoplasmic reticulum is the first element in the chain of the laser response. Specifically, it was found that the IP3 signaling pathway is primarily responsible for the observed effect upon exposure to the 450 nm ns laser pulse. This conclusion is based on the impact IP3R receptors had on fluorescence intensity, number of peaks, and time onset. Additionally, we found that channel inhibitors located at the endoplasmic reticulum are critical in determining the onset of the calcium response (2-APB, RR) and the concentration of the ion itself (2-APB) following ns laser stimulation. In regard to extracellular calcium release, we also conclude that TRPA1 and TRPV4 are not important for the response magnitude but contribute to the calcium dynamics. In particular, TRPA1 is not relevant for the response to occur but possibly could be involved in its duration. On the other hand, TRPV4 appears to mediate the initiation of the response and may play a key role

https://doi.org/10.1021/acs.jpcb.4c03251
J. Phys. Chem. B 2024, 128, 7966−7977

in the initiation of the calcium pathway elicited by nanosecond laser stimulation.

The results highlight, for the first time, the possibility of targeted excitation of diverse calcium signaling pathways in astrocytes at low-light intensity levels. The significant increase in astrocytic response upon the introduction of nanosecond-pulsed light establishes the utilization of the nanosecond laser as an area of continued interest. This finding underscores the potential of nanosecond-pulsed light in the advancement of therapeutic approaches.

In order to extend the application of imaging astrocytes, entangled two-photon light was explored as a lower-intensity alternative to nanosecond-pulsed light. The development of entangled two-photon absorption (ETPA) imaging is significant, as it paves the way for more reliable and physiologically controlled experimental conditions in fundamental neuroscience research. This is combined with a higher spatial resolution offered by entangled photon imaging.[46] For the first time, we present that ETPA imaging can be used to image astrocyte structures in vitro. Our results reveal the capacity to capture astrocytes at the single-cell level with 818 nm two-photon quantum-entangled light. Figure 7 shows the environment of the entangled image and the isolated astrocyte captured with a 409 nm, classical one-photon light. When referencing the quantum-entangled image to the classical image, it is apparent that quantum-entangled light accurately captures the cell morphology. In Figure 7, yellow and red represent areas of high fluorescence intensity, in contrast to the purple areas of lower fluorescence output. In light of this discovery, we present unique tools to study astrocytes and collectively extend the knowledge of astrocyte's interaction with light.

■ ASSOCIATED CONTENT

Supporting Information

The supporting information is available free of charge at https://pubs.acs.org/doi/10.1021/acs.jpcb.4c03251.

Additional experimental details pertaining to the astrocyte experiments, including the number of animals used, experimental trials, replicate trials, and recorded cells; information regarding the dye selection and fluorescent properties; the entangled two-photon laser setup; a schematic and a written description that explain the imaging technique and configuration of the entangled two-photon microscope (PDF)

■ AUTHOR INFORMATION

Corresponding Authors

Valentina Benfenati − *Istituto per la Sintesi Organica e Fotoreattività, Consiglio Nazionale delle Ricerche, 40129 Bologna, Italy*; Email: valentina.benfenati@isof.cnr.it

Theodor Goodson, III − *Department of Chemistry, University of Michigan, Ann Arbor, Michigan 48109, United States*; orcid.org/0000-0003-2453-2290; Email: tgoodson@umich.edu

Authors

Diletta Spennato − *Istituto per la Sintesi Organica e Fotoreattività, Consiglio Nazionale delle Ricerche, 40129 Bologna, Italy*

Josephine Leone − *Department of Chemistry, University of Michigan, Ann Arbor, Michigan 48109, United States*

Carolyn Gundhardt − *Department of Chemistry, University of Michigan, Ann Arbor, Michigan 48109, United States*

Oleg Varnavski − *Department of Chemistry, University of Michigan, Ann Arbor, Michigan 48109, United States*

Roberta Fabbri − *Istituto per la Sintesi Organica e Fotoreattività, Consiglio Nazionale delle Ricerche, 40129 Bologna, Italy*

Marco Caprini − *Dipartimento di Farmacia e Biotecnologie, Università di Bologna, 40126 Bologna, Italy*

Roberto Zamboni − *Istituto per la Sintesi Organica e Fotoreattività, Consiglio Nazionale delle Ricerche, 40129 Bologna, Italy*

Complete contact information is available at: https://pubs.acs.org/10.1021/acs.jpcb.4c03251

Author Contributions

#D.S. and J.L. are co-first authors. D.S., C.G., J.L., O.V., and P.J., performed most of the experimental work with the microscope. R.F. contributed to analyses of caclium imaging data, statistics and revised the figures. M.C. provided facilities, know how and knowledge to prepare primary rat neocortical astrocytes, R.Z. contributed to the discussion, co-supported with fundings the research. T.G. III and V.B. designed the concepts beyond this work, coordinate the research provide fundings. All authors contributed to discussions. All authors have given their approval to the final version of the manuscript.

Notes

The authors declare no competing financial interest.

■ ACKNOWLEDGMENTS

This work was supported by the Air Force Office of Scientific Research (AFOSR) Projects FA9550-20-1-0380, FA9550-20-1-0386, and FA9550-23-1-0736. This study was also supported by PRIN-PNRR-2022 (P2022Z27NS—Nanotechnological interfaces and devices enabling selective control of ion and water channels dynamics—NANODYN).

■ REFERENCES

(1) Varnavski, O.; Gunthardt, C.; Rehman, A.; Luker, G. D.; Goodson, T. Quantum Light-Enhanced Two-Photon Imaging of Breast Cancer Cells. *J. Phys. Chem. Lett.* **2022**, *13*, 2772−2781.

(2) Villabona-Monsalve, J. P.; Burdick, R. K.; Goodson, T. I. Measurements of Entangled Two-Photon Absorption in Organic Molecules with CW-Pumped Type-I Spontaneous Parametric Down-Conversion. *J. Phys. Chem. C* **2020**, *124*, 24526−24532.

(3) Kim, H.; Keller, B.; Ho-Wu, R.; et al. Enacting Two-Electron Transfer from a Double-Triplet State of Intramolecular Singlet Fission. *J. Am. Chem. Soc.* **2018**, *140*, 7760−7763.

(4) Villabona-Monsalve, J. P.; Varnavski, O.; Palfey, B. A.; Goodson, T. Two-Photon Excitation of Flavins and Flavoproteins with Classical and Quantum Light. *J. Am. Chem. Soc.* **2018**, *140*, 14562−14566.

(5) Aloisio, L.; Moschetta, M.; Boschi, A.; et al. Insight on the Intracellular Supramolecular Assembly of DTTO: A Peculiar Example of Cell-Driven Polymorphism. *Adv. Mater.* **2023**, *35*, No. 2302756.

(6) Thompson, A. C.; Stoddart, P. R.; Jansen, E. D. Optical Stimulation of Neurons. *Curr. Mol. Imaging* **2015**, *3*, 162−177.

(7) Berglund, K.; Stern, M. A.; Gross, R. E.Bioluminescence-Optogenetics. *Advances in Experimental Medicine and Biology*; Springer, 2021; Vol. *1293*, pp 281−293.

(8) Rial Verde, E. M.; Zayat, L.; Etchenique, R.; Yuste, R. Photorelease of GABA with Visible Light Using an Inorganic Caging Group. *Front. Neural Circuits* **2008**, *2*, No. 2, DOI: 10.3389/neuro.04.002.2008.

(9) Raos, B. J.; Graham, E. S.; Unsworth, C. P. Nanosecond UV lasers stimulate transient Ca2+ elevations in human hNT astrocytes. *J. Neural Eng.* **2017**, *14*, No. 035001.
(10) Shapiro, M. G.; Homma, K.; Villarreal, S.; Richter, C.-P.; Bezanilla, F. Infrared light excites cells by changing their electrical capacitance. *Nat. Commun.* **2012**, *3*, No. 736.
(11) Allen, N. J.; Lyons, D. A. Glia as architects of central nervous system formation and function. *Science* **2018**, *362*, 181−185.
(12) Fields, R. D.; Stevens-Graham, B. New insights into neuron-glia communication. *Science* **2002**, *298*, 556−562.
(13) Verkhratsky, A.; Nedergaard, M.; Hertz, L. Why are astrocytes important? *Neurochem. Res.* **2015**, *40*, 389−401.
(14) Buskila, Y.; Bellot-Saez, A.; Morley, J. W. Generating Brain Waves, the Power of Astrocytes. *Front. Neurosci.* **2019**, *13*, No. 1125, DOI: 10.3389/fnins.2019.01125.
(15) Chung, W.-S.; Allen, N. J.; Eroglu, C. Astrocytes Control Synapse Formation, Function, and Elimination. *Cold Spring Harbor Perspect. Biol.* **2015**, *7*, No. a020370.
(16) Escalada, P.; Ezkurdia, A.; Ramírez, M. J.; Solas, M. Essential Role of Astrocytes in Learning and Memory. *Int. J. Mol. Sci.* **2024**, *25*, No. 1899.
(17) Maiolo, L.; Guarino, V.; Saracino, E.; et al. Glial Interfaces: Advanced Materials and Devices to Uncover the Role of Astroglial Cells in Brain Function and Dysfunction. *Adv. Healthcare Mater.* **2021**, *10*, No. 2001268.
(18) Bazargani, N.; Attwell, D. Astrocyte calcium signaling: the third wave. *Nat. Neurosci.* **2016**, *19*, 182−189.
(19) Wang, X.; Lou, N.; Xu, Q.; et al. Astrocytic Ca2+ signaling evoked by sensory stimulation in vivo. *Nat. Neurosci.* **2006**, *9*, 816−823.
(20) Benfenati, V.; Ferroni, S. Water transport between CNS compartments: functional and molecular interactions between aquaporins and ion channels. *Neuroscience* **2010**, *168*, 926−940.
(21) Ahmadpour, N.; Kantroo, M.; Stobart, J. L. Extracellular Calcium Influx Pathways in Astrocyte Calcium Microdomain Physiology. *Biomolecules* **2021**, *11*, No. 1467.
(22) Stobart, J. L.; Ferrari, K. D.; Barrett, M. J.; et al. Cortical Circuit Activity Evokes Rapid Astrocyte Calcium Signals on a Similar Timescale to Neurons. *Neuron* **2018**, *98*, 726.e4−735.e4.
(23) Ozoran, H.; Srinivasan, R. Astrocytes and Alpha-Synuclein: Friend or Foe? *J. Parkinson's Dis.* **2023**, *13*, 1289−1301.
(24) Stoklund Dittlau, K.; Freude, K. Astrocytes: The Stars in Neurodegeneration? *Biomolecules* **2024**, *14*, No. 289.
(25) Butenko, O.; Dzamba, D.; Benesova, J.; et al. The increased activity of TRPV4 channel in the astrocytes of the adult rat hippocampus after cerebral hypoxia/ischemia. *PLoS One* **2012**, *7*, No. e39959.
(26) Zhao, Y.; Zhang, Y.; Liu, X.; et al. Photostimulation of astrocytes with femtosecond laser pulses. *Opt. Express* **2009**, *17*, 1291−1298.
(27) Zhao, Y.; Zhang, Y.; Zhou, W.; et al. Characteristics of calcium signaling in astrocytes induced by photostimulation with femtosecond laser. *J. Biomed. Opt.* **2010**, *15*, No. 035001.
(28) Cayce, J. M.; Bouchard, M. B.; Chernov, M. M.; et al. Calcium imaging of infrared-stimulated activity in rodent brain. *Cell Calcium* **2014**, *55*, 183−190.
(29) Borrachero-Conejo, A. I.; Adams, W. R.; Saracino, E.; et al. Stimulation of water and calcium dynamics in astrocytes with pulsed infrared light. *FASEB J.* **2020**, *34*, 6539−6553.
(30) Li, S.; Graham, E. S.; Unsworth, C. P. Extracellular ATP release predominantly mediates Ca2+ communication locally in highly organised, stellate-Like patterned networks of adult human astrocytes. *PLoS One* **2023**, *18*, No. e0289350.
(31) Hashmi, J. T.; Huang, Y.; Sharma, S. K.; et al. Effect of Pulsing in Low-Level Light Therapy. *Lasers Surg. Med.* **2010**, *42*, 450−466.
(32) Gao, Y.; Liu, C.; Xie, Y.; et al. Can Nanosecond Laser Achieve High-Performance Perovskite Solar Modules with Aperture Area Efficiency Over 21%? *Adv. Energy Mater.* **2022**, *12*, No. 2202287.
(33) Komin, N.; Moein, M.; Ellisman, M. H.; Skupin, A. Multiscale Modeling Indicates That Temperature Dependent [Ca2+]i Spiking in Astrocytes Is Quantitatively Consistent with Modulated SERCA Activity. *Neural Plast.* **2015**, No. 683490.
(34) Schmidt, E.; Oheim, M. Infrared Excitation Induces Heating and Calcium Microdomain Hyperactivity in Cortical Astrocytes. *Biophys. J.* **2020**, *119*, 2153−2165.
(35) Keller, B.; Cai, Z.; Muthike, A. K.; et al. Investigating the Optical Properties of Thiophene Additions to s-Indacene Donors with Diketopyrrolopyrrole, Isoindigo, and Thienothiophene Acceptors. *J. Phys. Chem. C* **2018**, *122*, 27713−27733.
(36) Liu, Z.; Zou, Y.; Sun, Y.; et al. Effects of Nanosecond Pulsed Electric Fields in Cell Vitality, Apoptosis, and Proliferation of TPC-1 Cells. *Anal. Cell. Pathol.* **2021**, *2021*, No. 9913716.
(37) Stockley, J. H.; Evans, K.; Matthey, M.; et al. Surpassing light-induced cell damage in vitro with novel cell culture media. *Sci. Rep.* **2017**, *7*, No. 849.
(38) Degl'Innocenti, E.; Dell'Anno, M. T. Human and mouse cortical astrocytes: a comparative view from development to morphological and functional characterization. *Front. Neuroanat.* **2023**, *17*, No. 1130729.
(39) Durkee, C. A.; Araque, A. Diversity and Specificity of Astrocyte-neuron Communication. *Neuroscience* **2019**, *396*, 73−78.
(40) Park, K.; Lee, S. J. Deciphering the star codings: astrocyte manipulation alters mouse behavior. *Exp. Mol. Med.* **2020**, *52*, 1028−1038.
(41) Zhou, B.; Zuo, Y.-X.; Jiang, R.-T. Astrocyte morphology: Diversity, plasticity, and role in neurological diseases. *CNS Neurosci. Ther.* **2019**, *25*, 665−673.
(42) Mellor, N. G.; Chung, S. A.; Graham, E. S.; Day, B. W.; Unsworth, C. P. Eliciting calcium transients with UV nanosecond laser stimulation in adult patient-derived glioblastoma brain cancer cells in vitro. *J. Neural Eng.* **2023**, *20*, No. 066026.
(43) Ebtehaj, Z.; Hatef, A.; Malekmohammad, M.; Soltanolkotabi, M. Computational Modeling and Validation of Thermally Induced Electrical Capacitance Changes for Lipid Bilayer Membranes Irradiated by Pulsed Lasers. *J. Phys. Chem. B* **2018**, *122*, 7319−7331.
(44) Moreau, D.; Lefort, C.; Pas, J.; et al. Infrared neural stimulation induces intracellular Ca2+ release mediated by phospholipase C. *J. Biophotonics* **2018**, *11*, No. e201700020, DOI: 10.1002/jbio.201700020.
(45) Varnavski, O.; Giri, S. K.; Chiang, T. M.; Zeman, C. J., IV; Schatz, G. C.; Goodson, T., III Colors of entangled two-photon absorption. *Proc. Natl. Acad. Sci. U.S.A.* **2023**, *120*, No. e2307719120.
(46) Varnavski, O.; Pinsky, B.; Goodson, T., III Entangled Photon Excited Fluorescence in Organic Materials: An Ultrafast Coincidence Detector. *J. Phys. Chem. Lett.* **2017**, *8*, 388−393.
(47) Lee, D.-I.; Goodson, T. Entangled Photon Absorption in an Organic Porphyrin Dendrimer. *J. Phys. Chem. B* **2006**, *110*, 25582−25585.
(48) Guzman, A. R.; Harpham, M. R.; Süzer, Ö.; Haley, M. M.; Goodson, T. G., III Spatial Control of Entangled Two-Photon Absorption with Organic Chromophores. *J. Am. Chem. Soc.* **2010**, *132*, 7840−7841.
(49) McCarthy, K. D.; de Vellis, J. Preparation of separate astroglial and oligodendroglial cell cultures from rat cerebral tissue. *J. Cell Bio.* **1980**, *85* (3), 890−902.